European Radiology (2019) 29:2535–2544
https://doi.org/10.1007/s00330-018-5804-5

BREAST

Differentiation of triple-negative breast cancer from other subtypes through whole-tumor histogram analysis on multiparametric MR imaging

Tianwen Xie[1] · Qiufeng Zhao[2] · Caixia Fu[3] · Qianming Bai[4] · Xiaoyan Zhou[4] · Lihua Li[5] · Robert Grimm[6] · Li Liu[1] · Yajia Gu[1] · Weijun Peng[1]

Received: 28 May 2018 / Revised: 31 August 2018 / Accepted: 25 September 2018 / Published online: 6 November 2018

Abstract

Purpose To identify triple-negative (TN) breast cancer imaging biomarkers in comparison to other molecular subtypes using multiparametric MR imaging maps and whole-tumor histogram analysis.

Materials and methods This retrospective study included 134 patients with invasive ductal carcinoma. Whole-tumor histogram-based texture features were extracted from a quantitative ADC map and DCE semi-quantitative maps (washin and washout). Univariate analysis using the Student's *t* test or Mann–Whitney *U* test was performed to identify significant variables for differentiating TN cancer from other subtypes. The ROC curves were generated based on the significant variables identified from the univariate analysis. The AUC, sensitivity, and specificity for subtype differentiation were reported.

Results The significant parameters on the univariate analysis achieved an AUC of 0.710 (95% confidence interval [CI] 0.562, 0.858) with a sensitivity of 63.6% and a specificity of 73.1% at the best cutoff point for differentiating TN cancers from Luminal A cancers. An AUC of 0.763 (95% CI 0.608, 0.917) with a sensitivity of 86.4% and a specificity of 72.2% was achieved for differentiating TN cancers from human epidermal growth factor receptor 2 (HER2) positive cancers. Also, an AUC of 0.683 (95% CI 0.556, 0.809) with a sensitivity of 54.5% and a specificity of 83.9% was achieved for differentiating TN cancers from non-TN cancers. There was no significant feature on the univariate analysis for TN cancers versus Luminal B cancers.

Conclusions Whole-tumor histogram-based imaging features derived from ADC, along with washin and washout maps, provide a non-invasive analytical approach for discriminating TN cancers from other subtypes.

Key Points

- *Whole-tumor histogram-based features on MR multiparametric maps can help to assess biological characterization of breast cancer.*
- *Histogram-based texture analysis may predict the molecular subtypes of breast cancer.*
- *Combined DWI and DCE evaluation helps to identify triple-negative breast cancer.*

Keywords Triple-negative breast cancer · Magnetic resonance imaging · Classification · Immunologic subtyping · ROC curve

Tianwen Xie and Qiufeng Zhao contributed equally to this work and are co-first authors for this study.

Electronic supplementary material The online version of this article (https://doi.org/10.1007/s00330-018-5804-5) contains supplementary material, which is available to authorized users.

✉ Weijun Peng
pengweijun2017@163.com

[1] Department of Radiology, Fudan University Shanghai Cancer Center, No. 270 Dong'an Road, Shanghai 200032, People's Republic of China

[2] Department of Radiology, Longhua Hospital, Shanghai University of Traditional Chinese Medicine, Shanghai, People's Republic of China

[3] MR Applications Development, Siemens Shenzhen Magnetic Resonance Ltd., Shenzhen, People's Republic of China

[4] Department of Pathology, Fudan University Shanghai Cancer Center, Shanghai, People's Republic of China

[5] Institute of Biomedical Engineering and Instrumentation, Hangzhou Dianzi University, Hangzhou, People's Republic of China

[6] MR Application Predevelopment, Siemens Healthineers, Erlangen, Germany

Abbreviations

ADC	Apparent diffusion coefficient
AUC	Area under the curve
DCE	Dynamic contrast-enhanced imaging
DWI	Diffusion-weighted imaging
ER	Estrogen receptor
HER2	Human epidermal growth factor receptor 2
IDC	Invasive ductal carcinoma
IHC	Immunohistochemical
PR	Progesterone receptor
SD	Standard deviation
SI	Signal intensity
TN	Triple-negative

Introduction

Breast cancer is a heterogeneous disease that presents with varied tumor behavior and may require a variety of therapeutic interventions to improve the overall outcome [1]. Immunohistochemical (IHC) subtypes including the estrogen receptor (ER), progesterone receptor (PR), human epidermal growth factor receptor 2 (HER2), and Ki-67 labeling index are routinely analyzed to select the appropriate therapy [2]. Triple-negative (TN) breast cancer, lacking ER, PR, and HER2 receptors, is an aggressive disease with outcomes inferior to those of other subtypes [3–5].

Multiparametric magnetic resonance (MR) imaging with dynamic contrast-enhanced imaging (DCE) and diffusion-weighted imaging (DWI) has been applied to identify molecular subtype and therapeutic response prediction in patients with TN cancers [6–8]. Some groups have reported that TN cancers initially possess a rapid washin enhancement and a washout pattern and have poor prognostic factors [9, 10]. Moreover, Youk JH et al reported a rim enhancement on DCE and a higher apparent diffusion coefficient (ADC) value on DWI that were significantly associated with TN cancers [7]. However, Uematsu et al showed that a persistent enhancement pattern was significantly associated with TN cancers [11].

Computer algorithms can evaluate the spatial distributions of pixel gray-levels on medical images, which provide an imaging-based phenotype [12]. However, for breast MR imaging, texture analysis has moved beyond diagnosing cancer [13, 14] to understanding tumor biology, such as subtype differentiation [15–18]. Authors of a pilot study proposed the use of texture indices from DCE images in differentiating TN breast cancer from other subtypes of breast cancer [15]. Kim et al [19] and Choi et al [20] reported that ADC histogram analysis could facilitate the identification of TN cancers. However, to our knowledge, no published studies have investigated the texture analysis using both DCE and DWI images for the breast cancer subtype classification. Therefore, the purpose of our study was to determine the feasibility of texture analysis based on histogram analysis and to compare TN cancers to Luminal A cancers, Luminal B cancers, and HER2 positive cancers using quantitative ADC and DCE semiquantitative maps (washin and washout).

Materials and methods

Patients

This retrospective study was approved by our institutional review board, which issued a waiver of informed consent. The study included a total of 159 consecutive patients with core needle-biopsy proven invasive ductal carcinoma (IDC). All patients underwent pre-operative MR examinations with DCE and DWI sequences between February 2016 and May 2017. The exclusion criteria included the following: patients treated with a prior history of malignancy ($n = 5$), patients with lesions smaller than 1 cm ($n = 16$), patients with artifacts or poor fat suppression on DWI ($n = 3$), and patients with body-movement artifact among DCE phases ($n = 1$). For the 20 patients with multicentric or multifocal tumors, the tumors with the largest sizes according to the first phase of postcontrast images were analyzed. Therefore, a total of 134 women (mean age, 51 years; age range, 24–84 years), with a total of 134 tumors were enrolled.

MR imaging

MR imaging was performed on a MAGNETOM Skyra 3 T MR system (Siemens Healthineers, Erlangen, Germany) with a dedicated 16-channel phased-array breast coil. The breast MR examinations included a fat-suppressed T2-weighted 2D fast spin-echo, a T1-weighted 3D gradient-echo, as well as DWI and DCE protocols in transversal plane.

The DWI was executed before contrast-agent injection using a fat-suppressed single-shot echo-planar imaging (EPI) sequence with the following parameters: TR/TE = 3000/54 ms; field of view = 34 cm; matrix = 220 × 220; slice thickness = 6 mm; interslice gap = 1.5 mm; number of slices = 16; fat saturation mode of spectral adiabatic inversion recovery (SPAIR); b value = 0, 400, and 800 s/mm^2 with number of averages = 3, 4, 5 respectively; EPI factor = 96; receive bandwidth = 1516 Hz/Pixel; parallel acquisition (GRAPPA) with acceleration factor of 3; acquisition time = 2:09 min. ADC map was inline calculated by the scanner integrated Syngo software (Siemens Healthineers, Erlangen, Germany) using all b values with a mono-exponential fit.

DCE was obtained using a fat-suppressed T1-weighted 3D fast spoiled gradient-echo sequence before and five times continuously after the contrast agent injection. A rapid bolus of gadolinium contrast agent (Magnevist, Bayer HealthCare Pharmaceuticals Inc., Wayne, USA)

was injected intravenously at a dose of 0.1 mmol per kilogram of body weight with an injection rate of 2 ml/s followed by a 20 mL saline flush. The scan parameters were as following: TR/TE = 4.5/1.6 ms; field of view = 34 cm; flip angle = 10°; matrix = 384 × 384; slice thickness = 1.5 mm; number of slices = 80; duration = 60s. Pixel-wise washin (the steepness of the ascending curve) and washout (the steepness of the descending curve) parametric maps were inline generated with the Syngo software after acquisition (the inline postprocessing detail for the calculation of DCE parametric maps was given in the supplementary material). Washin and washout were defined in the equations respectively, using the following equations: washin = $[(SI_{max} - SI_0) \times 100\%]/[SI_0 \times (T_{peak} - T_{arrive})]$, and washout = $[(SI_{last} - SI_{max}) \times 100\%]/[SI_{max} \times (T_{end} - T_{peak})]$, where SI_0, SI_{max}, and SI_{last} are the non-enhanced signal intensity (SI), the maximum contrast-enhanced SI within 2 min and the last contrast-enhanced SI, respectively [16, 21]. T_{peak} and T_{end} were defined as the time points that corresponded to SI_{max} and SI_{last}. T_{arrive} was the time point from the contrast injection to the appearance of contrast in the breast.

Histogram analysis

Two radiologists (X.T.W. and Z.Q.F. with 2 and 8 years of experience in breast MR imaging, respectively) who were blinded to the pathologic results but were aware of the IDC diagnosis, reviewed the MR images, and the largest lesion (in case of multicentric or multifocal tumors) was selected by consensus.

Histogram analysis was performed with the prototype MR Multiparameter Analysis software (Siemens Healthineers, Erlangen, Germany) by the radiologist (X.T.W.). The analysis of ADC map and the DCE-derived parametric maps were executed separately. The processing workflow included the following four steps:

a. Data loading. MR data (DWI images with *b* value of 0 s/mm^2, ADC maps, the first postcontrast images, washin and washout maps) were loaded to the software.
b. Seed points drawing. For ADC map analysis, foreground and background seed points were manually drawn inside and outside of the tumor respectively on the three multiplane reconstruction (MPR) planes of the ADC map, with DWI and DCE images as reference. While for DCE map analysis, the seed points were drawn on the postcontrast images.
c. Segmentation. The segmentation of the whole tumor was executed basing on these seed points with a random-walker algorithm [22]. Manual adjustment for the segmentation was done if necessary. For DCE maps, 3D-segmented volumes that were created on the postcontrast images were propagated to washin and washout maps automatically.
d. Histogram analysis. Histogram analysis for the whole tumor on the parametric maps was performed and the statistical parameters were extracted, included mean, standard deviation (SD), median, percentiles (5th and 95th), skewness (a measure of asymmetry of the probability distribution), and kurtosis (a measure of the shape of the probability distribution).

The steps of b, c, and d were illustrated in Fig. 1.

Histopathologic analysis

Axillary lymph node metastasis, and expression statuses of ER, PR, and HER2 receptor status, and Ki-67 were routinely recorded. ER status was considered positive if more than 1% of the nuclei stained positive. Positive HER2 expression was defined by IHC scores of 3+ or FISH amplification with a ratio ≥ 2.0. Ki-67 of 14% was considered a positive expression. The IHC subtype of the tumor was classified as Luminal A (ER and/or PR positive, HER2 negative, and Ki-67 < 14%), Luminal B (ER and/or PR positive, HER2 negative, and Ki-67 ≥ 14% or ER and/or PR positive, HER2 positive, irrespective of Ki-67 expression), HER2 positive (ER and PR negative, HER2 positive), and TN (ER negative, PR negative, and HER2 negative) [2].

Statistical analysis

Descriptive analysis including frequencies for categorical variables, and mean and range for continuous variables, was used to present patients' clinical characteristics. Chi-square test and analysis of variance were then employed to compare the differences in clinical characteristics. With the univariate analyses, the significant feature selection was performed by the Student's *t* test when normally distributed or Mann-Whitney *U* test when not normally distributed. The analysis was repeated four times: TN group vs. Luminal A group, TN group vs. Luminal B group, TN group vs. HER2 positive group, and TN group vs. non-TN group (including Luminal A group, Luminal B group and HER2 positive group). The receiver operating characteristic (ROC) curves using logistic regression model for each pair-wise subtype differentiation involving TN group were generated based on the significant variables identified from the univariate analysis. In addition, the area under the curve (AUC), accuracy, sensitivity, and specificity at the best cutoff point were reported. All analyses were performed using SPSS (version 22; IBM, Armonk, NY, USA). A *p* value less than 0.05 was considered a statistically significant difference.

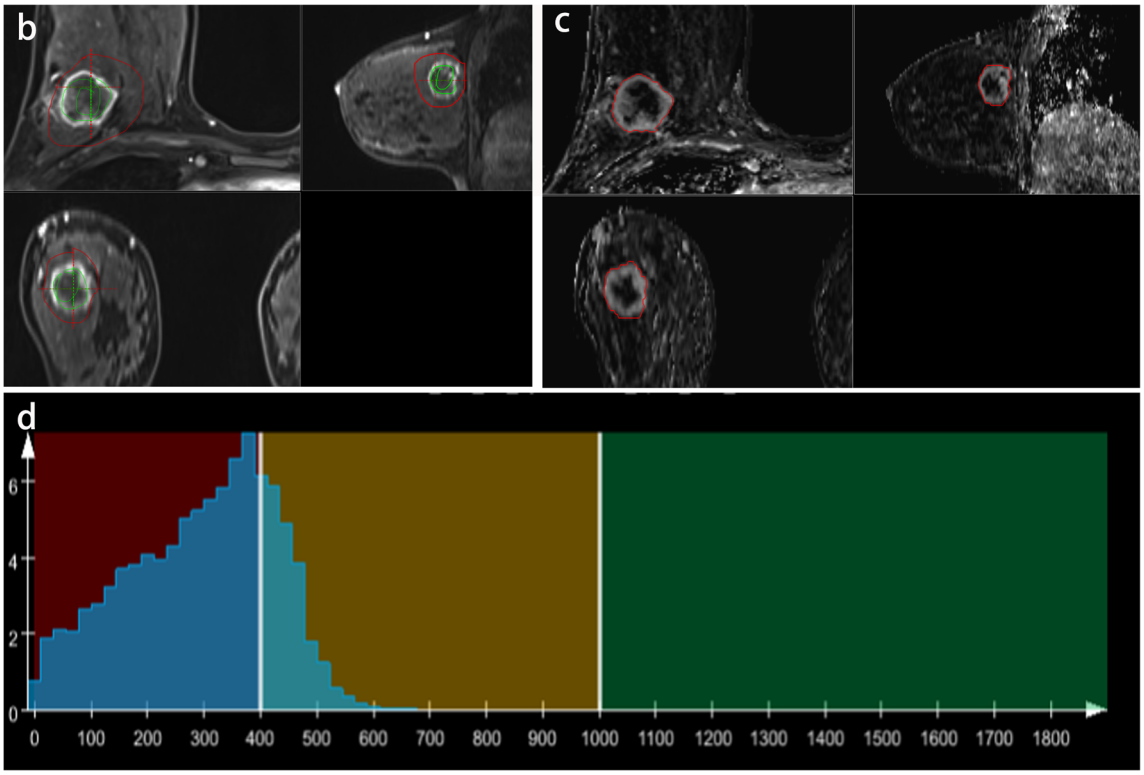

Fig. 1 Workflow for the histogram analysis (take the histogram analysis for washin maps as an example). Foreground and background seed points were manually drawn inside (green color) and outside (red color) on the three multiplane reconstruction planes of the postcontrast images (**b**). The 3D segmentation created on the postcontrast images was propagated to washin maps (**c**). Then, the histogram for washin maps was generated (**d**)

Results

Patient characteristics

The clinical pathological characteristics of patients were listed in Table 1. Of the 134 invasive breast cancers examined in this study, 22 (16.4%) were TN cancer, 26 (19.4%) were Luminal A cancer, 68 (50.7%) were Luminal B cancer, and 18 (13.4%) were HER2 positive cancer (Figs. 2 and 3). The axillary lymph node involvement status showed significant difference among breast subtypes ($p = 0.007$). No significant differences were found across groups regarding age or menopause status ($p = 0.607$ and $p = 0.378$). There is a significant difference in the lesion size among groups ($p = 0.038$).

Table 1 Clinicopathologic characteristics

Characteristic	Luminal A ($n = 26$)	Luminal B ($n = 68$)	HER2 positive ($n = 18$)	Triple-negative ($n = 22$)	p value
Age					0.607^
> 50 years at diagnosis	12	29	8	13	
≤50 years at diagnosis	14	39	10	9	
Menopausal status					0.378^
Peri- or postmenopausal	11	29	8	14	
Premenopausal	15	38	10	8	
Unknown	0	1	0	0	
Lesion size (mm)*	18 (11–47)	25 (10–80)	21 (10–43)	24 (13–39)	*0.038*#
Axillary lymph node					*0.007*^
Negative	21	30	7	13	
Positive	5	38	11	9	

HER2 human epidermal growth factor receptor 2

The p value listed in italics indicates a significant difference

*Data are means, with ranges in parentheses. The p value with # refers to analysis of variance, and the p values with ^ refer to chi-square test

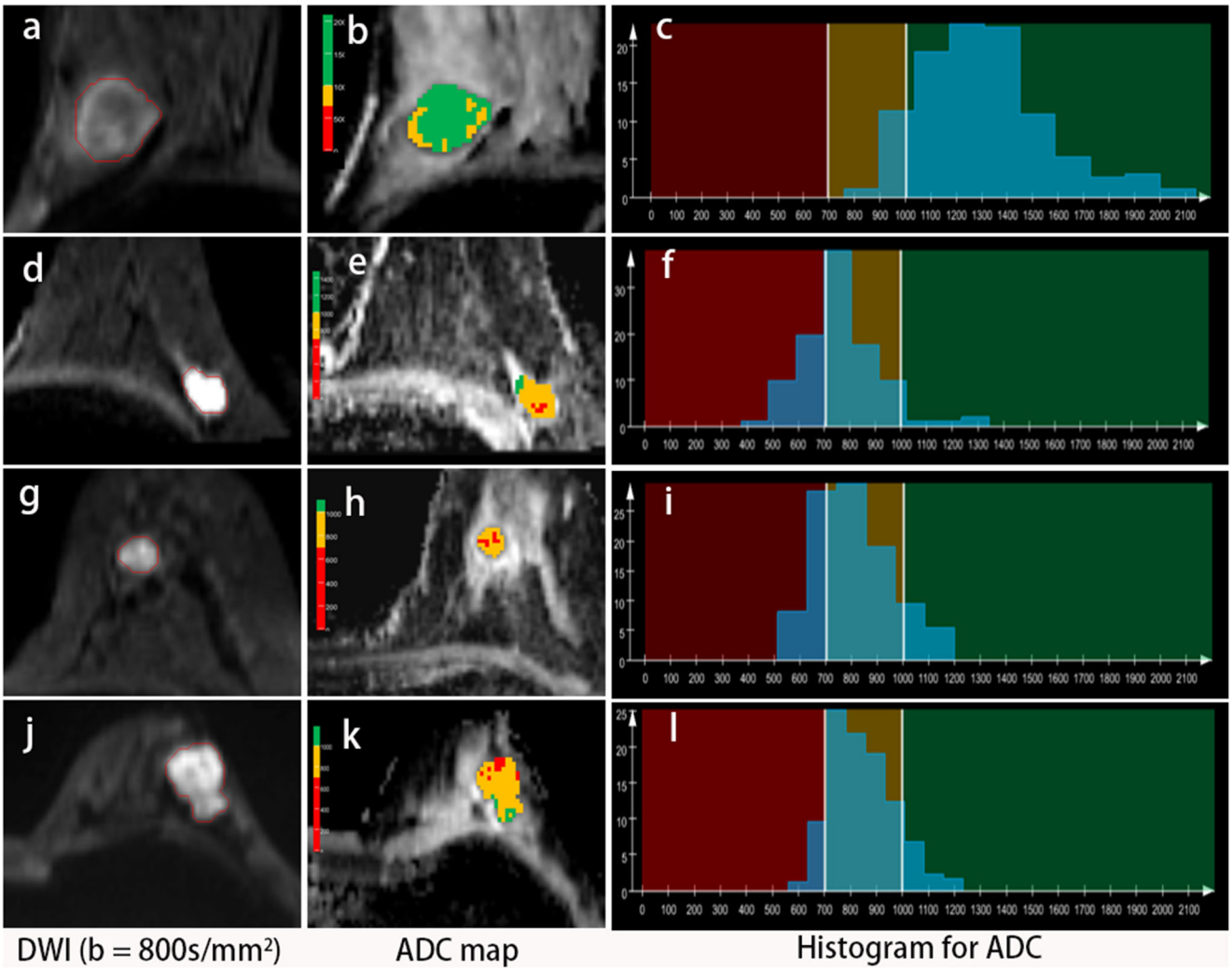

Fig. 2 A 46-year-old female with triple-negative breast cancer (**a**, **b**, **c**), a 60-year-old female with Luminal A breast cancer (**d**, **e**, **f**), a 57-year-old female with Luminal B breast cancer, and a 47-year-old female with human epidermal growth factor receptor 2 (HER2) positive breast cancer. DWI with b 800 s/mm^2 (**a**, **d**, **g**, **j**), ADC map overlaid with color maps of ADC values (**b**, **e**, **h**, **k**) and histogram of whole-tumor ADC map (**c**, **f**, **i**, **l**) of four subtypes

Univariate analysis and performance of subtype differentiation

The univariate analysis of extracted features is shown in Table 2, and their performances based on subtype differentiation are shown in Table 3 and Fig. 4.

When comparing the TN group to the Luminal A group, the ADC_{SD} and $ADC_{95th\ percentile}$ were significantly higher in the TN group than those in the Luminal A group ($p = 0.015$, 0.019, respectively). In addition, the $washin_{5th\ percentile}$ ($p = 0.029$) was significantly lower in the TN group than those in Luminal A group. The subtype differentiation between the TN group and the Luminal A group yielded an AUC of 0.710 (95% CI 0.562, 0.858), an accuracy of 68.8%, a sensitivity of 63.6%, and a specificity of 73.1%.

The TN group compared to the Luminal B group revealed no significant differences based on the extracted features ($p =$ 0.085–0.107). Of note, a subtype classification between the TN group and Luminal B group was not performed.

With regard to the differences between the TN group and the HER2 positive group, the $washin_{mean}$, $washin_{median}$, $washin_{5th\ percentile}$, and $washin_{95th\ percentile}$ of the TN group were significantly lower than those of the HER2 positive group ($p = 0.015$, 0.013, 0.020, 0.036, respectively). In addition, a higher $washout_{median}$ for TN cancers compared to the HER2 positive cancers was found ($p = 0.021$). We obtained an AUC of 0.763 (95% CI 0.608, 0.917), an accuracy of 80.0%, a sensitivity of 86.4%, and a specificity of 72.2% for the subtype differentiation between the TN group and the HER2 positive group.

When comparing the TN group to the non-TN group, TN cancers showed a significantly higher ADC_{mean} relative to the non-TN group ($p = 0.042$). In addition, the non-TN groups had a higher $washin_{mean}$, $washin_{median}$, and $washin_{5th\ percentile}$

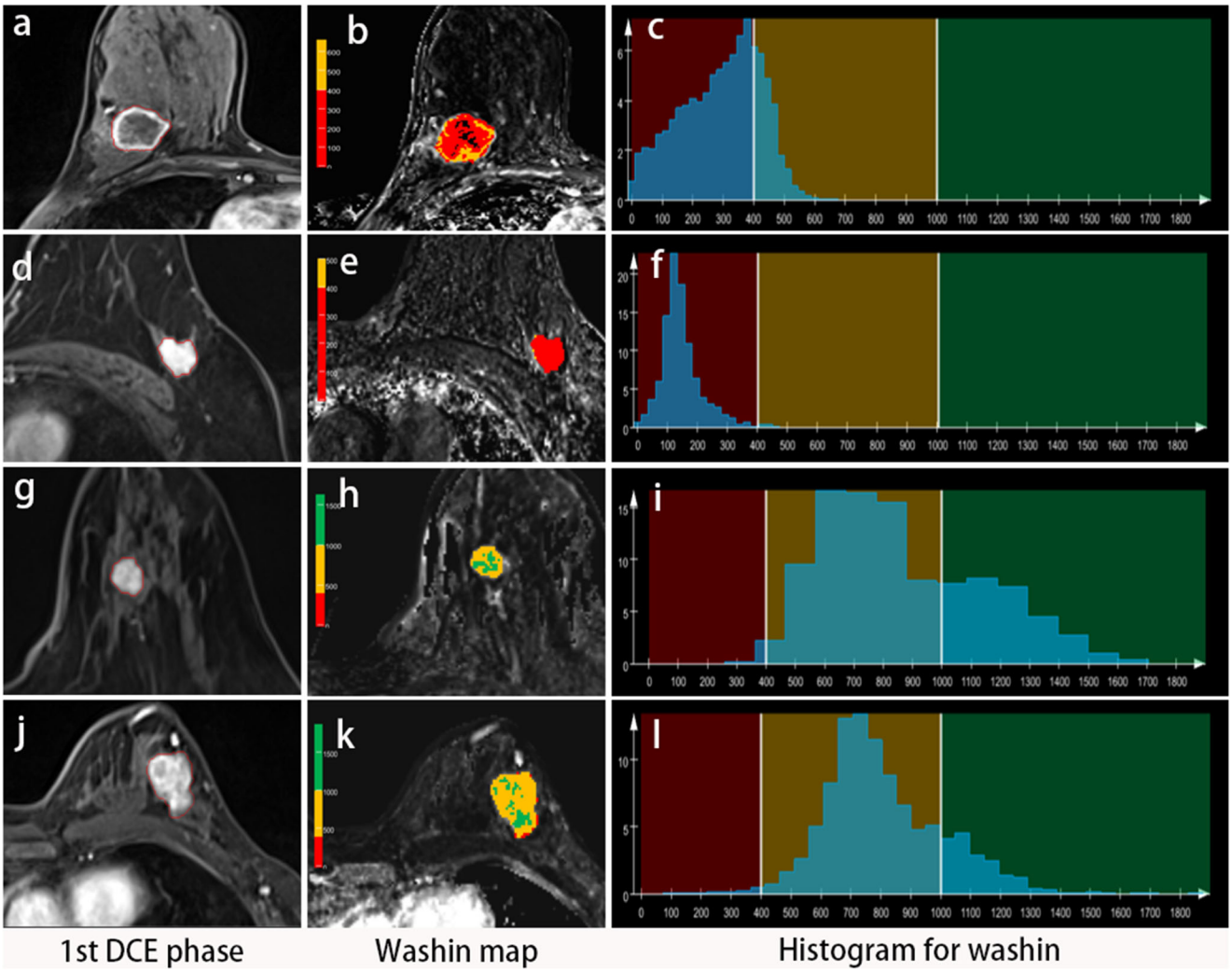

Fig. 3 A 46-year-old female with triple-negative breast cancer (**a**, **b**, **c**), a 60-year-old female with Luminal A breast cancer (**d**, **e**, **f**), a 57-year-old female with Luminal B breast cancer, and a 47-year-old female with human epidermal growth factor receptor 2 (HER2) positive breast cancer. The first DCE phase (**a**, **d**, **g**, **j**), washin map overlaid with color maps of washin values (**b**, **e**, **h**, **k**) and histogram of whole-tumor washin map (**c**, **f**, **i**, **l**) of four subtypes

values ($p = 0.034$, $p = 0.033$, $p = 0.024$, respectively) compared to the TN group. For subtype differentiation between the TN group and the non-TN group, we obtained an AUC of 0.683 (95% CI 0.556, 0.809), an accuracy of 79.1%, a sensitivity of 54.5%, and a specificity of 83.9%.

Discussion

Our study found that computer-extracted features from ADC along with washin and washout maps can be assessed as potential biomarkers for identifying TN cancers. Although this is a preliminary work, whole-tumor histogram-based imaging phenotypes from MR multiparametric maps may provide a non-invasive tool for assessing biological characteristics and heterogeneity of breast cancers.

DWI detects the Brownian motion of water molecules and provides a quantitative ADC parameter. The ADC closely reflects the microenvironment of tumor structures, such as tumor cellularity, water content, the amount of fibrous stroma, and cell membrane integrity [23]. Recently, ADC has been used more for identifying molecular subtypes of breast cancer. However, the results were not in consensus [7, 8, 19, 24, 25], which might be due to different *b* values, magnetic field, and ROI definition (2D or 3D, including or excluding necrosis portion, et al). Our study found that $ADC_{95th\ percentile}$ and ADC_{SD} values of TN tumors were higher than those of Luminal A tumors. In addition, the ADC_{mean} value of TN tumors was higher than that of non-TN tumors. A possible explanation for this finding is that TN tumors were more frequently associated with intra-tumoral necrosis [11, 25]. In our study, there were 11 of 22 TN tumors exhibiting rim enhancement (intra-tumoral necrosis) on the first postcontrast phase.

Table 2 Univariate analysis of histogram-based parameters for differentiating TN from other subtypes

	Variable	TN	Luminal A	*p* value[1]	Luminal B	*p* value[2]	HER2 positive	*p* value[3]	Non-TN	*p* value[4]
ADC	Mean (10^{-3} mm^2/s)	1.093 ± 0.250	0.954 ± 0.141	0.086	1.005 ± 0.208	0.107	1.039 ± 0.136	0.849	0.999 ± 0.185	*0.042*
	SD (10^{-3} mm^2/s)	0.219 ± 0.110	0.155 ± 0.060	*0.015*	0.202 ± 0.081	0.429	0.181 ± 0.070	0.207	0.188 ± 0.077	0.106
	Median (10^{-3} mm^2/s)	1.071 ± 0.248	0.937 ± 0.135	0.098	0.989 ± 0.211	0.131	1.022 ± 0.139	0.935	0.982 ± 0.186	0.055
	5th percentile (10^{-3} mm^2/s)	0.769 ± 0.150	0.718 ± 0.123	0.209	0.710 ± 0.168	0.151	0.772 ± 0.129	0.917	0.722 ± 0.153	0.197
	95th percentile (10^{-3} mm^2/s)	1.482 ± 0.413	1.229 ± 0.232	*0.019*	1.374 ± 0.323	0.206	1.356 ± 0.211	0.514	1.337 ± 0.293	0.160
	Skewness	0.490 ± 0.553	0.334 ± 0.450	0.286	0.387 ± 0.581	0.466	0.347 ± 0.513	0.406	0.368 ± 0.539	0.336
	Kurtosis	0.415 ± 0.991	0.286 ± 0.757	0.611	0.432 ± 1.002	0.945	0.419 ± 0.884	0.991	0.396 ± 0.926	0.930
Washin	Mean (100%/min)	49.1 ± 23.2	64.6 ± 32.7	0.069	58.6 ± 22.1	0.085	68.3 ± 24.4	*0.015*	61.6 ± 25.3	*0.034*
	SD (100%/min)	16.7 ± 9.1	16.9 ± 9.0	0.943	19.0 ± 10.5	0.353	20.5 ± 8.7	0.184	18.8 ± 9.9	0.363
	Median (100%/min)	48.0 ± 22.5	64.0 ± 32.1	0.056	57.2 ± 21.8	0.092	67.1 ± 24.1	*0.013*	60.4 ± 25.0	*0.033*
	5th percentile (100%/min)	24.0 ± 19.3	38.1 ± 23.5	*0.029*	31.0 ± 16.1	0.094	37.3 ± 14.2	*0.020*	33.7 ± 18.0	*0.024*
	95th percentile (100%/min)	77.7 ± 35.4	92.9 ± 46.9	0.219	91.0 ± 36.4	0.138	103.2 ± 38.6	*0.036*	93.4 ± 39.3	0.085
	Skewness	0.577 ± 0.679	0.316 ± 0.651	0.181	0.699 ± 1.113	0.631	0.594 ± 0.924	0.949	0.593 ± 1.000	0.944
	Kurtosis	2.008 ± 4.113	1.148 ± 2.481	0.377	3.751 ± 8.566	0.361	3.556 ± 7.433	0.409	3.115 ± 7.438	0.499
Washout	Mean (100%/min)	1.7 ± 2.5	−0.2 ± 7.3	0.142	1.1 ± 3.3	0.445	0.4 ± 1.5	0.055	0.7 ± 4.4	0.292
	SD (100%/min)	5.4 ± 2.6	5.1 ± 2.1	0.631	6.3 ± 3.2	0.272	5.9 ± 2.0	0.492	5.9 ± 2.8	0.433
	Median (100%/min)	1.3 ± 2.5	−0.6 ± 7.5	0.263	0.7 ± 3.3	0.388	−0.4 ± 1.8	*0.021*	0.2 ± 0.5	0.259
	5th percentile (100%/min)	−6.1 ± 3.1	−7.6 ± 8.4	0.457	−7.5 ± 5.1	0.240	−7.5 ± 2.3	0.138	−7.5 ± 5.7	0.274
	95th percentile (100%/min)	11.0 ± 6.1	8.3 ± 6.2	0.134	11.0 ± 4.4	0.999	10.7 ± 3.3	0.854	10.3 ± 4.9	0.566
	Skewness	0.820 ± 0.868	1.089 ± 3.092	0.695	1.236 ± 2.419	0.450	1.315 ± 2.003	0.302	1.215 ± 2.511	0.468
	Kurtosis	6.974 ± 21.979	13.392 ± 61.745	0.646	16.560 ± 50.144	0.388	11.181 ± 34.137	0.640	14.960 ± 50.590	0.470

TN triple-negative, *HER2* human epidermal growth factor receptor 2, *ADC* apparent diffusion coefficient, *SD* standard deviation

p value[1] : difference in values between TN group and Luminal A group. *p* value[2] : difference in values between TN group and Luminal B group. *p* value[3] : difference in values between TN group and HER2 positive group. *p* value[4] : difference in values between TN group and non-TN positive group. The *p* value listed in italics indicates a significant difference

Table 3 AUC, accuracy, specificity, and specificity for differentiating TN from Luminal A, HER2 positive, and non-TN breast cancers

	TN vs Luminal A	TN vs HER2 positive	TN vs non-TN
AUC (95% CI)	0.710 (0.562, 0.858)	0.763 (0.608, 0.917)	0.683 (0.556, 0.809)
Accuracy	68.8%	80.0%	79.1%
Sensitivity	63.6%	86.4%	54.5%
Specificity	73.1%	72.2%	83.9%

AUC area under the curve, *TN* triple-negative, *HER2* human epidermal growth factor receptor 2, *AUC* areas under the curve, *CI* confidence interval

Tumor cellularity can decrease in necrotic areas, resulting in an increased ADC value [26, 27].

DCE can be used to extract morphologic and kinetic features, which have been found to be associated with a different tumor grade, histologic type, and molecular subtype [28–31]. Established characteristics of malignant breast lesions are a rapid washin enhancement followed by a washout [32]. In our study, various washin-related parameters in TN cancers were significantly lower than those in Luminal A, HER2 positive, and non-TN cancers, especially in the HER2 positive group. $Washin_{mean}$, $washin_{median}$, $washin_{5th\ percentile}$, and $washin_{95th\ percentile}$ of HER2 positive cancers are also higher than those of TN cancers. These findings were consistent with recent studies [31, 33], which showed that the percent volume of TN breast cancers demonstrating rapid early contrast uptake was significantly decreased compared to the HER2 positive subtype. Since HER2 expression correlates with an overexpression of vascular endothelial growth factor (VEGF), which can increase angiogenesis [34–36]. Also, tumor heterogeneity may influence imaging parameters of the whole volume analysis. Intra-tumoral necrosis—predominant in TN tumors—may lead to a lower $washin_{mean}$, $washin_{median,}$ and $washin_{5th\ percentile}$ values compared to HER2 positive and non-TN tumors along with a lower $washin_{5th\ percentile}$ value compared to luminal A tumors. In addition, researchers found that TN tumors were significantly associated with a persistent enhancement pattern [11]. This may explain our findings that a $washout_{median}$ of TN tumor was higher than that of the HER2 tumor. To our best knowledge, there are no other similar breast cancer histogram analysis studies that involve washin and washout values.

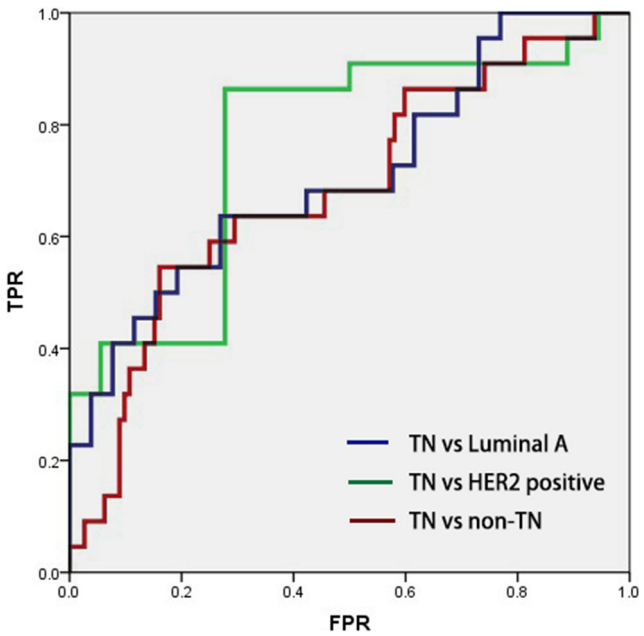

Fig. 4 Receiver operating characteristic (ROC) curve for differentiation of TN group versus Luminal A group using ADC_{SD}, $ADC_{95th\ percentile}$, and $washin_{5th\ percentile}$ features, ROC curve for differentiation of TN group versus HER2 positive group using $washin_{mean}$, $washin_{median}$, $washin_{5th\ percentile}$, $washin_{95th\ percentile}$, and $washout_{median}$ features, ROC curve for differentiation of TN group versus non-triple-negative group using ADC_{mean}, $washin_{mean}$, $washin_{median}$, and $washin_{5th\ percentile}$ features. FPR false positive rate, TPR true positive rate, AUC areas under the curve, TN triple-negative, HER2 human epidermal growth factor receptor 2

TN breast cancer lacks expression of all three receptors (ER, PR, and HER2) and is known to have biologically and clinically aggressive features [3]. Biological characteristics regarding tumor cellularity derived from ADC and contrast enhancement kinetics from DCE parameters may be used as potential biomarkers for TN cancer identification. In our study, the subtype differentiations between TN group and Luminal A group, between TN group and HER2 positive group, and between TN group and non-TN group yielded AUCs of 0.710 (95% CI 0.562, 0.858), 0.763 (95% CI 0.608, 0.917), and 0.683 (95% CI 0.556, 0.809), respectively.

Our study had several strengths because our results indicate that histogram analysis of MR multiparametric maps for assessing the biological information and heterogeneity of cancer can be potentially used as surrogate imaging markers for subtype classifications. In addition, semi-automated segmentation and volumetric analysis may mitigate the variability of manual single-slice or multislices measurements [37, 38]. Finally, inline parametric maps and histogram-based image features can be understood and interpreted widely by physicians without a high degree of mathematical knowledge.

However, our study had several limitations. First, this is a retrospective, single-institution study based on a single MR system. Secondly, the histologic type was limited to only IDC, and breast cancers with different subtypes were numerically unbalanced. Also, small tumors with a size less than 1 cm

were excluded due to a relatively large slice thickness and a limited in-plane resolution of DWI images. Future validation using readout-segmented DWI [39] with a capability of assessing smaller lesions is required. Thirdly, the current processing workflow is not optimized for clinical routine. To become more widely adopted, automatic co-registration of the image contrasts as well as optimized segmentation tools will be required. Finally, we extracted only the first-order histogram-based features. However, previous studies reported that histogram-based features were ranked higher than the higher-order texture features [40, 41]. Further studies are required to compare the performance of histogram-based and higher-order features for subtype differentiation.

In summary, our study revealed that the whole-tumor histogram-based features from the combined use of quantitative ADC map and DCE semi-quantitative maps (washin and washout) may provide a more sophisticated biological characterization of breast cancer, which could be potentially useful for discrimination of breast cancer molecular subtypes.

Funding This study has received funding by the National Natural Science Foundation of China (61731008).

Compliance with ethical standards

Guarantor The scientific guarantor of this publication is Weijun Peng.

Conflict of interest The authors of this manuscript declare no relationships with any companies, whose products or services may be related to the subject matter of the article.

Statistics and biometry No complex statistical methods were necessary for this paper.

Informed consent This study is retrospective study and does not require informed consent.

Ethical approval Institutional Review Board approval was obtained.

Methodology
- Retrospective
- Diagnostic or prognostic study
- Performed at one institution

References

1. Wu JM, Fackler MJ, Halushka MK et al (2008) Heterogeneity of breast cancer metastases: comparison of therapeutic target expression and promoter methylation between primary tumors and their multifocal metastases. Clin Cancer Res 14:1938–1946
2. Goldhirsch A, Wood WC, Coates AS et al (2011) Strategies for subtypes–dealing with the diversity of breast cancer: highlights of the St. Gallen international expert consensus on the primary therapy of early breast cancer 2011. Ann Oncol 22:1736–1747
3. Dent R, Trudeau M, Pritchard KI et al (2007) Triple-negative breast cancer: clinical features and patterns of recurrence. Clin Cancer Res 13:4429–4434
4. Liedtke C, Mazouni C, Hess KR et al (2008) Response to neoadjuvant therapy and long-term survival in patients with triple-negative breast cancer. J Clin Oncol 26:1275–1281
5. Cleator S, Heller W, Coombes RC (2007) Triple-negative breast cancer: therapeutic options. Lancet Oncol 8:235–244
6. Loo CE, Straver ME, Rodenhuis S et al (2011) Magnetic resonance imaging response monitoring of breast cancer during neoadjuvant chemotherapy: relevance of breast cancer subtype. J Clin Oncol 29:660–666
7. Youk JH, Son EJ, Chung J, Kim JA, Kim EK (2012) Triple-negative invasive breast cancer on dynamic contrast-enhanced and diffusion-weighted MR imaging: comparison with other breast cancer subtypes. Eur Radiol 22:1724–1734
8. Kato F, Kudo K, Yamashita H et al (2016) Differences in morphological features and minimum apparent diffusion coefficient values among breast cancer subtypes using 3-tesla MRI. Eur J Radiol 85:96–102
9. Chen JH, Agrawal G, Feig B et al (2007) Triple-negative breast cancer: MRI features in 29 patients. Ann Oncol 18:2042–2043
10. Koo HR, Cho N, Song IC et al (2012) Correlation of perfusion parameters on dynamic contrast-enhanced MRI with prognostic factors and subtypes of breast cancers. J Magn Reson Imaging 36:145–151
11. Uematsu T, Kasami M, Yuen S (2009) Triple-negative breast cancer: correlation between MR imaging and pathologic findings. Radiology 250:638–647
12. Zhang B, Chang K, Ramkissoon S et al (2017) Multimodal MRI features predict isocitrate dehydrogenase genotype in high-grade gliomas. Neuro Oncol 19:109–117
13. Gibbs P, Turnbull LW (2003) Textural analysis of contrast-enhanced MR images of the breast. Magn Reson Med 50:92–98
14. Sinha S, Lucas-Quesada FA, DeBruhl ND et al (1997) Multifeature analysis of Gd-enhanced MR images of breast lesions. J Magn Reson Imaging 7:1016–1026
15. Agner SC, Rosen MA, Englander S et al (2014) Computerized image analysis for identifying triple-negative breast cancers and differentiating them from other molecular subtypes of breast cancer on dynamic contrast-enhanced MR images: a feasibility study. Radiology 272:91–99
16. Chaudhury B, Zhou M, Goldgof DB et al (2015) Heterogeneity in intratumoral regions with rapid gadolinium washout correlates with estrogen receptor status and nodal metastasis. J Magn Reson Imaging 42:1421–1430
17. Mazurowski MA, Zhang J, Grimm LJ, Yoon SC, Silber JI (2014) Radiogenomic analysis of breast cancer: luminal B molecular subtype is associated with enhancement dynamics at MR imaging. Radiology 273:365–372
18. Waugh SA, Purdie CA, Jordan LB et al (2016) Magnetic resonance imaging texture analysis classification of primary breast cancer. Eur Radiol 26:322–330
19. Kim EJ, Kim SH, Park GE et al (2015) Histogram analysis of apparent diffusion coefficient at 3.0t: correlation with prognostic factors and subtypes of invasive ductal carcinoma. J Magn Reson Imaging 42:1666–1678
20. Choi Y, Kim SH, Youn IK, Kang BJ, Park WC, Lee A (2017) Rim sign and histogram analysis of apparent diffusion coefficient values on diffusion-weighted MRI in triple-negative breast cancer: comparison with ER-positive subtype. PLoS One. https://doi.org/10.1371/journal.phone.0177903
21. Harms SE (1999) Technical report of the international working group on breast MRI. J Magn Reson Imaging 10:979
22. Grady L (2006) Random walks for image segmentation. IEEE Trans Pattern Anal Mach Intell 28:1768–1783
23. Koh DM, Collins DJ (2007) Diffusion-weighted MRI in the body: applications and challenges in oncology. AJR Am J Roentgenol 188:1622–1635

24. Martincich L, Deantoni V, Bertotto I et al (2012) Correlations between diffusion-weighted imaging and breast cancer biomarkers. Eur Radiol 22:1519–1528
25. Liu S, Ren R, Chen Z et al (2015) Diffusion-weighted imaging in assessing pathological response of tumor in breast cancer subtype to neoadjuvant chemotherapy. J Magn Reson Imaging 42:779–787
26. Padhani AR, Liu G, Koh DM et al (2009) Diffusion-weighted magnetic resonance imaging as a cancer biomarker: consensus and recommendations. Neoplasia 11:102–125
27. Park SH, Moon WK, Cho N et al (2010) Diffusion-weighted MR imaging: pretreatment prediction of response to neoadjuvant chemotherapy in patients with breast cancer. Radiology 257:56–63
28. Rahbar H, Partridge SC, Demartini WB et al (2012) In vivo assessment of ductal carcinoma in situ grade: a model incorporating dynamic contrast-enhanced and diffusion-weighted breast MR imaging parameters. Radiology 263:374–382
29. Narisada H, Aoki T, Sasaguri T et al (2006) Correlation between numeric gadolinium-enhanced dynamic MRI ratios and prognostic factors and histologic type of breast carcinoma. AJR Am J Roentgenol 187:297–306
30. Schmitz AM, Loo CE, Wesseling J, Pijnappel RM, Gilhuijs KG (2014) Association between rim enhancement of breast cancer on dynamic contrast-enhanced MRI and patient outcome: impact of subtype. Breast Cancer Res Treat 148:541–551
31. Blaschke E, Abe H (2015) MRI phenotype of breast cancer: kinetic assessment for molecular subtypes. J Magn Reson Imaging 42:920–924
32. Kuhl CK, Mielcareck P, Klaschik S et al (1999) Dynamic breast MR imaging: are signal intensity time course data useful for differential diagnosis of enhancing lesions? Radiology 211:101–110
33. Leong LC, Gombos EC, Jagadeesan J, Fook-Chong SM (2015) MRI kinetics with volumetric analysis in correlation with hormonal receptor subtypes and histologic grade of invasive breast cancers. AJR Am J Roentgenol 204:W348–W356
34. Brown LF, Berse B, Jackman RW et al (1995) Expression of vascular permeability factor (vascular endothelial growth factor) and its receptors in breast cancer. Hum Pathol 26:86–91
35. Kumar R, Yarmand-Bagheri R (2001) The role of HER2 in angiogenesis. Semin Oncol 28:27–32
36. Esteva FJ, Hortobagyi GN (2004) Prognostic molecular markers in early breast cancer. Breast Cancer Res 6:109–118
37. Lambregts DM, Beets GL, Maas M et al (2011) Tumour ADC measurements in rectal cancer: effect of ROI methods on ADC values and interobserver variability. Eur Radiol 21: 2567–2574
38. Stoutjesdijk MJ, Futterer JJ, Boetes C, van Die LE, Jager G, Barentsz JO (2005) Variability in the description of morphologic and contrast enhancement characteristics of breast lesions on magnetic resonance imaging. Invest Radiol 40:355–362
39. Robson MD, Anderson AW, Gore JC (1997) Diffusion-weighted multiple shot echo planar imaging of humans without navigation. Magn Reson Med 38:82–88
40. Sutton EJ, Dashevsky BZ, Oh JH et al (2016) Breast cancer molecular subtype classifier that incorporates MRI features. J Magn Reson Imaging 44:122–129
41. Kim JH, Ko ES, Lim Y et al (2017) Breast cancer heterogeneity: MR imaging texture analysis and survival outcomes. Radiology 282:665–675